Indian Journal of Biochemistry & Biophysics
Vol. 60, July 2023, pp. 545-554
DOI: 10.56042/ijbb.v60i7.4371

A microscopy study to distinguish the ultrastructural changes in the ciliated epithelium, type II pneumocytes, macrophages, and neutrophils of bronchoalveolar fluids after severe SARS-CoV-2 infection

Shikha Chaudhary, Ravi Prakash Yadav & Subhash Chandra Yadav*

Electron Microscope Facility, Department of Anatomy, All India Institute of Medical Sciences, New Delhi-110 029, Delhi, India

Received 05 May 2023; *revised 12 July 2023*

SARS-CoV-2 infection has an adverse effect on the functioning of various respiratory and hematopoietic cells in the bronchoalveolar fluid (BALF) resulting from ultrastructural alterations. These ultrastructural changes were directly corroborated to understand the altered function of these cells. These changes have been sparingly reported and it is important for understanding the biology of COVID-19. We have reported various ultrastructural alterations of ciliated epithelium, type II pneumocytes, macrophages, and neutrophils individually from the BALF of patients with severe COVID-19. Ultrastructural alterations depend on various conditions such as age, immunity, associated comorbidities, disease severity, and medication received by patients. The ciliated epithelium mostly contained viral-containing compartments, horseshoe-shaped mitochondria, necrosis, and double-membrane vesicles. Type II pneumocyte cells showed cytoplasmic vacuolization, loss of lamellar bodies, and the formation of viral inclusion bodies. The alveolar macrophages displayed increased size and number of phagocytic vacuoles containing viral particles (phagosomes) and vacuolated cytoplasm. Neutrophils showed cytoplasmic granularity, vacuolization, and the presence of extracellular traps. This study provides important insights into the cellular and morphological changes associated with COVID-19 in BALF cells.

Keywords: Bronchoalveolar fluids, Ciliated epithelium, Macrophages, Neutrophils, SARS-CoV-2, Type II pneumocytes

Coronavirus disease 2019 (COVID-19), caused by severe acute respiratory syndrome coronavirus 2 (SARS-CoV-2), has become a pandemic that poses a significant threat to global public health[1-3]. The virus primarily infects the respiratory tract and causes various clinical manifestations ranging from asymptomatic infection to severe acute respiratory distress syndrome (ARDS) and multiple organ failure[4-6].

Pathological and histological examinations have indicated that SARS-CoV-2 primarily targets the airways and lungs[7,8]. Recent studies have shown that COVID-19 patients exhibit characteristic changes in the ultrastructure and morphology of these lung cells[9]. Electron microscopy revealed the presence of coronavirus particles in the bronchial mucosal and type II pneumocytes[10]. Viral particles have been observed mainly in degenerated pneumocytes, in the endothelium, or freely circulating in the alveoli[11-13]. A recent study explored the effects of SARS-CoV-2 infection on the respiratory epithelial and inflammatory cells in BALF samples[14]. Immunofluorescence and ultrastructural findings in this study provided evidence of the interactions between viruses and host cells, the level of infection, and cellular changes in different lung cells[15].

Bronchoalveolar lavage fluid (BALF) from the lung is the primary source of all types of respiratory and infiltrated hematopoietic cells to study ultrastructural alterations[16,17]. However, direct cellular and ultrastructural changes have been sparingly reported to explore the effects of SARS-CoV-2 infection in the respiratory epithelial and inflammatory cells in BALF. Transmission and scanning electron microscopy, along with immunofluorescence studies, offer a direct and detailed exploration of SARS-CoV-2 infection in different bronchoalveolar fluid (BALF) cells, providing crucial evidence of cellular infection load and ultrastructural changes in affected patients[18]. Recently, we have explored ultrastructural alteration of various cell types, including ciliated epithelium, type II pneumocytes, macrophages, and neutrophils, within these BALF samples[19-21]. Microscopic analysis

*Correspondence:
Phone: +91-11-26549127, +91-9868126177 (Mob);
Fax: +91-1126588663/641
E-mail: subhashmbu@aiims. gov. in, subhashmbu@gmail. com

of BALF from old and young patients with or without comorbidities showed a distinction in the infection level and alterations in the ultrastructure of the respiratory epithelial and inflammatory cells[19]. In these studies, we have successfully demonstrated the levels of infection present in these diverse cell populations using *ex vivo* BALF samples collected from COVID-19 patients with acute respiratory distress syndrome (ARDS). The data obtained from these analyses contribute significantly to our understanding of the disease pathogenesis and the specific cellular targets affected by SARS-CoV-2 in severe cases[19].

In the current study, we have investigated the ultrastructural and morphological changes in the ciliated epithelium, type II pneumocytes, macrophages, and neutrophils from bronchoalveolar lavage fluid (BALF) samples obtained from COVID-19 patients. We used Immunofluorescence, scanning electron microscopy (SEM), and transmission electron microscopy (TEM) techniques. The study allows us to gain valuable insights into the cellular responses and ultrastructural alterations associated with severe SARS-CoV-2 infection in these specific cell types within the respiratory tract.

Material and Methods

Material

Osmium tetroxide was procured from Ted Pella, USA, Uranyl acetate from TAAB, UK, lead citrate from Ladd, polyclonal anti-SARS-CoV-2 specific primary antibody (Cat no. ab275759), and Alexa fluor-594 conjugated anti-rabbit secondary antibodies (Cat no. ab150080) from Abcam, Plc, UK. Hematoxylin, eosin, orange G., Scott's water, xylene, DPX, PBS, poly-L-lysin, epoxy embedding kit, Karnovsky's fixative (0.5% glutaraldehyde + 2.0 % paraformaldehyde), and DAPI were purchased from Sigma St. Louis, MO, USA). BSA, ethanol from HiMedia, and Triton X-100 were purchased from Fisher Scientific.

Methods

Ethics statement

After obtaining written consent from all patient representatives, experimental procedures were performed to collect BALF samples from severely SARS-CoV-2-infected and intubated patients. The study was conducted following ethical approval from the Institutional Ethics Committee (IEC), All India Institute of Medical Sciences (AIIMS), New Delhi, India (Ref. No. IEC-307/27.04.2020, RP-10/202).

Sample collection

BALF samples were collected from intubated SARS-CoV-2-positive patients in the COVID-19 intensive care unit (ICU), AIIMS, and New Delhi. All samples were collected from October 3, 2020, to January 31, 2021. The BALF sample (15-20mL) was primarily fixed in freshly prepared 20 ml, 2X Karnovsky's solution (final 1% glutaraldehyde + 4.0 % formaldehyde) in 0.2M phosphate buffer. The surface of the sample vials was sterilized with an alcohol/soap solution by incubating for 2 h at room temperature and then stored at 4°C in a COVID-19-designated refrigerator.

Sample processing for the cellular enrichment

After the primary fixation Karnovsky's fixative (0.5% glutaraldehyde + 2.0 % paraformaldehyde), the BALF sample was diluted ten times with 0.1 M NaCl solution and strained through a nylon mesh cell strainer with a 100 µM pore. The filtrate was centrifuged at 2500 rpm for 3 min in a swinging bucket. The cell pellets were washed 2-3 times for 10 min in PBS to remove excess mucus. The cellular content was enriched by centrifugation at 1200 g for 3 to 5 min and resuspended again in primary fixative A (0.5% glutaraldehyde 2.0% paraformaldehyde in 0.1 M PB buffer). The samples were processed for IF, SEM, and TEM.

Immunofluorescence using SARS-CoV-2 spike protein-specific antibody

BALF samples were washed three times with 0.1 M phosphate buffer, and smears were prepared using 10 to 12 µL of sample on poly-L-lysine coated glass slides and air-dried at RT Smears were permeabilized with PBST (0.1% Triton X-100 in 1X phosphate buffer saline, PBS) and blocked with 2 % BSA in PBS for 30 min. After blocking with BSA, the slides were incubated with the primary antibody (Abcam ab275759, polyclonal against S1 spike protein, dilution 1:500) for 4 h in a humid chamber at room temperature. After washing with PBS, a fluorophore-conjugated secondary antibody (Alexa fluor-594 conjugated anti-rabbit secondary antibody; Abcam, Cat No. - 150080; dilution 1:500) was added for 1 h at RT in the dark. The smears were washed with phosphate buffer, and DAPI (1 µg/mL) was added for 5 min. Excess DAPI was removed by washing with PBS, and smears were mounted with 90% glycerol. Fluorescence imaging was performed using a laser-scanning confocal microscope (Leica SP8, Germany).

Scanning electron microscopy

For SEM, BALF's enriched and primary fixed cellular components were osmicated, dehydrated with ethanol, critical point dried (E-3100, Quorum Tech), and mounted on double-sided tape on aluminum stubs. The stubs were sputter-coated with a gold-based sputter coater (HHV BT-150) for 180s. Electron micrographs were obtained using an EVO18 (Zeiss, Germany) SEM operated at 20 an accelerating voltage of 8-10, an average working distance with an SE detector, with magnifications ranging from 5,000 × to 30,000 ×.

Transmission electron microscopy

For TEM imaging, enriched cellular constituents of BALF were fixed using 2. 5% glutaraldehyde + 2.0% paraformaldehyde in 0.1 M phosphate buffer (PB). The fixed cellular pellets were washed with 0.1 M PB (pH 7. 4) and post-fixed with 1% osmium tetroxide in 0.1 M PB (pH 7. 4) for one hour (secondary fixation) at 4°C. The pellets were washed with distilled water for 2 h, and en bloc, staining was performed with 2% uranyl acetate in 50% ethanol. The samples were again washed with distilled water and dehydrated in an ethanol series (50%, 70%, 80%, 90%, and 100%). The dry pellets were infiltrated with toluene/resin and embedded in Araldite CY212 resin.

Results and Discussion

Ciliated epithelium

The ciliated epithelium (from nasal to bronchus) in the BALF of COVID-19 patients showed a higher presence of S-glycoprotein near the apical side (towards the basal bodies of cilia and microvilli) in comparison to other parts of the cells (Fig. 1). The Immunofluorescence generated from the S glycoprotein was also visible in these cells' microvilli (higher) and cilia (lesser). These cells showed a relatively lower intensity than the apical cell body (Fig. 1). The different sizes and shapes of the ciliated epithelium also indicated that these cells were unanimously infected with the virus from the nasal cavity to the bronchus (Fig. 1). The gradual decrease in the size of the ciliated epithelium (the elongated size of these cells decreases from nasal to bronchioles) provides direct confirmation of different zones of ciliated cells infected by the SARS-CoV-2 (Fig. 1). Some of the heavily infected cilia cells were observed without the nucleus (Fig. 1H & L).

Many ciliated epithelial cells were observed in the BALF samples by scanning electron microscopy. These cells showed intact microvilli and cilia on their apical surfaces (Fig. 2). Protrusions of viral-like structures were visible on the cilia of these cells.

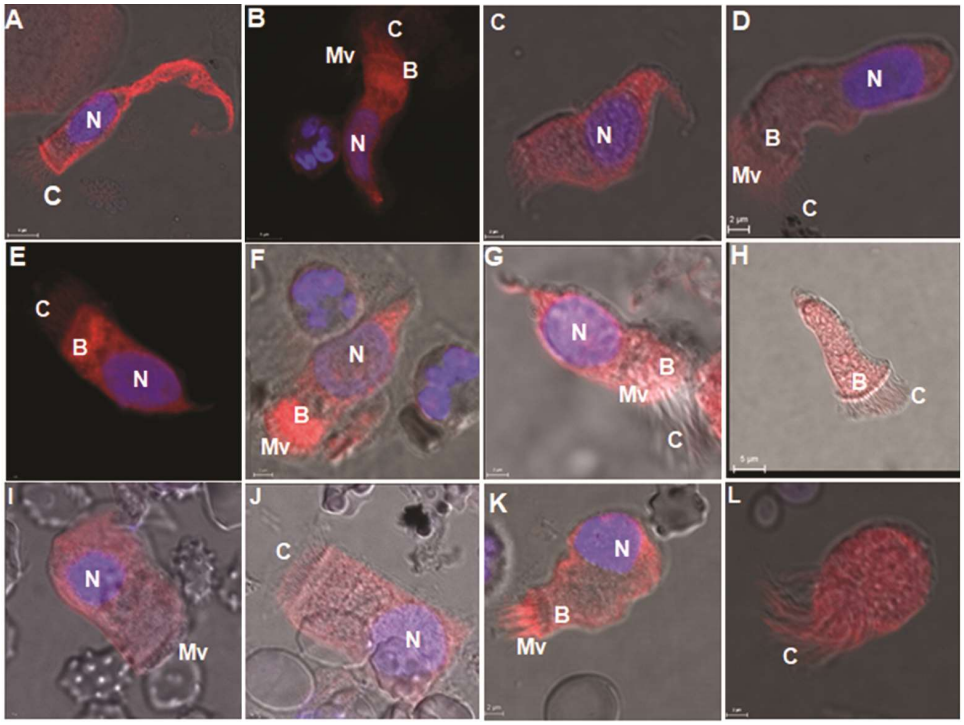

Fig. 1 — Immunofluorescence images of various types of ciliated epithelial cells (from nasal to bronchus from BALF of intubated COVID-19 patients. The size of the ciliated epithelium gradually reduces from the nasal cavity (a-d), and branchia to alveoli of the lung (e-l). Mv: Microvilli; N: Nucleus; B: Basal body; C: Cilia

These protrusions were similar to those observed on the surface of the plasma membranes of these cells (Fig. 2G). The protruding surface could result from the fusion of the virus with the cilia, leaving behind the fused membrane patches. At a higher magnification, these protrusions matched the size (60–80 nm) of the SARS-CoV-2 virus on the cilia (Fig. 2A and D-F). However, in the healthy samples, this protrusion was absent (Fig. 2B-C). Extracellular virions were mostly localized to microvilli and cilia. Reduced cilia density and shorter cilia length were observed compared to those in healthy individuals. In addition, some cilia were broken or disorganized. This is likely due to the destruction of ciliated epithelial cells by the virus, leading to the impairment of the mucociliary clearance mechanism of the respiratory tract (Fig. 2).

Transmission electron microscopy revealed viral fusion with the plasma membrane, demonstrating the site of entry of these viruses (Fig. 3). Intact intracellular virions were found within ciliated cells in compartments with a single membrane called viral-containing compartments (VCs) (Fig. 3). The mitochondria were distorted with a horseshoe shape, dense, and deformed. Many cells showed necrotic characteristics (Fig. 3). Endoplasmic reticulum (ER)-derived structures, such as virus replication sites or double-membrane vesicles (DMVs denoted as D), were also observed[22]. These DMVs are located in small double-membrane spherules reported to contain double-stranded RNA[23,24]. Lysosomes containing the viral particles in the host cell were also indicative of post-viral replication (Fig. 3)[25]. The viral replication machinery, including DMVs, convoluted membranes, and viral-containing compartments (VCs), were observed in many cells (Fig. 3)[22,26]. Many extracellular viruses, intracellular endosomal matured viruses, and non-coated viruses were also observed (Fig. 3). The identifiable feature of SARS-CoV-2 virions is the presence of nucleocapsid contents in the viral lumen, as an electron-dense punctate pattern was also observed in many cell images. This feature was distinguishable from clathrin-coated and intraluminal vesicles, as previously reported by Pinto *et al*. (Fig. 3)[27]. Most of the VCs contained virions that were not coated with the crown of S glycoprotein on the surface, indicating the maturation phase of this virus (Fig. 3). Many basal bodies (B) were visible, even though these cells showed degenerative cilia as an adverse effect of viral infection. These findings

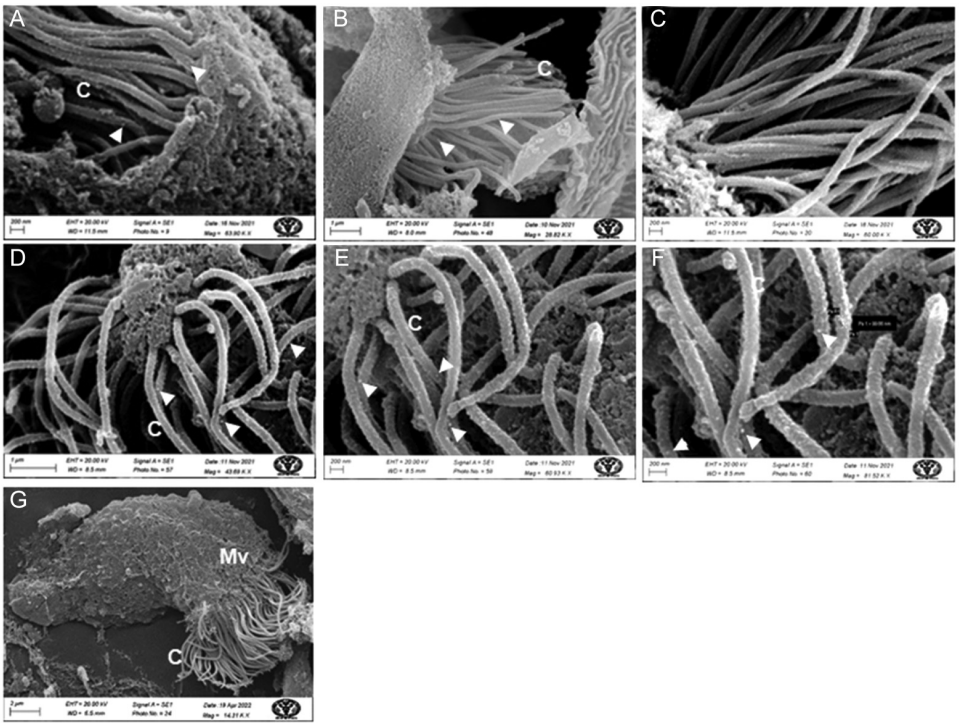

Fig. 2 — Scanning electron microscopy of the apical portion of the ciliated cells from the BALF samples of severely infected COVID-19 patients. The cilia were infected with the SARS-CoV-2 virus, which is indicated by the protrusion (a, d, e & f). An epithelial cell with microvilli was also represented (g). This is direct evidence of the presence of SARS-CoV-2 in the cilia, which was also shown in the immunofluorescence study. C: Cilia, Mv: Microvilli

suggested that ciliated epithelium is a crucial target for SARS-CoV-2 infection, with the virus showing a preference for the apical side and microvilli. These cell changes in cilia structure and density likely contribute to the impairment of mucociliary clearance, potentially leading to respiratory complications in COVID-19 patients.

Type II pneumocytes

The ultrastructural changes in type II pneumocyte cells from bronchoalveolar lavage fluid (BALF) samples with severe COVID-19 showed strong Immunofluorescence in the plasma membrane and cytoplasm, indicating the presence of viral particles in the cytoplasm and plasma membrane. This was confirmed by an immunofluorescence (IF) study using S protein-specific antibodies to confirm the presence of mature viruses or S proteins. Some of the cells showed apoptotic nucleases in IF.

SEM imaging examined the ultrastructural changes in type II pneumocyte cells from BALF samples of severely infected patients. SEM analysis revealed the distinctive morphology, presence of lamellar bodies, and microvilli on the surface with numerous virus-like particles (Fig. 4). In addition, the infected cells showed morphological changes such as swelling and detachment from the extracellular matrix. The infected cells appeared flattened and had fewer microvilli on their surface (Fig. 4). The cell membranes of infected cells also appeared to be damaged, with numerous irregularities and blebs[19] (Fig. 4). Giant multinucleated type II pneumocytes with large nucleoli were observed, consistent with our previous study[21] and other groups[11,28].

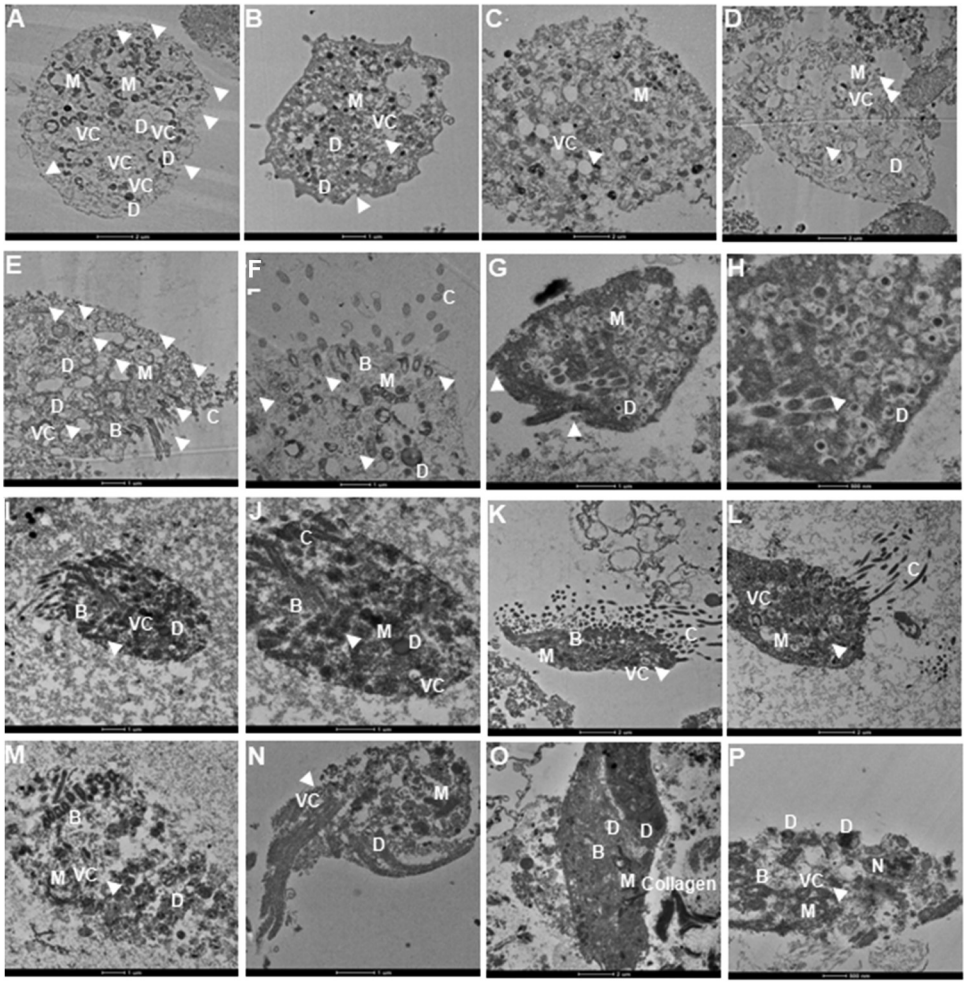

Fig. 3 — Transmission Electron Microscopy of ciliated epithelium with the basal bodies as identifiable features. The ciliated epithelium was identified by the presence of a ciliary basal body and cilia in the section. Viral-containing compartments (VCs) was observed in many ciliary cells and double-membrane vesicles (DMVs denoted as D) as replication site. N: Nucleus, M: Mitochondria, B: Basal Body, C: Cilia, arrowhead: virus-like particles

TEM imaging of type II pneumocyte cells from COVID-19 patients showed marked ultrastructural changes, including cytoplasm vacuolization, loss of lamellar bodies, and formation of viral inclusion bodies (Fig. 4). Recently, we also identified the presence of giant lamellar bodies in patients with severe COVID-19 with ARDS-like symptoms[29]. We observed widespread cytoplasmic vacuolization in these cells, with varying sizes and shapes, often filled with electron-dense material (Fig. 4). These vacuoles merge to form large cytoplasmic spaces. We also observed an increased number of autophagosomes and autolysosomes in the cytoplasm of type II pneumocyte cells, consistent with our previous TEM analysis, indicating autophagy pathway activation[19] (Fig. 4). These particles have a diameter of approximately 100-120 nm and a characteristic corona-like structure. We also observed increased apoptotic bodies in the cytoplasm of pneumocyte type II cells from COVID-19 patients (Fig. 4). These bodies are characterized by condensed chromatin and fragmented cytoplasm, indicating cell death by apoptosis. Some cells showed characteristic large-size surfactant granules or giant lamellar granules (LG)[29].

Macrophages

Macrophages are essential components of the innate immune system and serve as the first line of defense against invading pathogens, including viruses. Their ability to phagocytose and eliminate pathogens makes them crucial players in the immune response to viral infections. The macrophages from the BALF of COVID-19 patients showed increased size and number of phagocytic vacuoles containing viral particles (phagosomes) and vacuolated cytoplasm. Additionally, we observed a higher number of apoptotic macrophages in the BALF of COVID-19

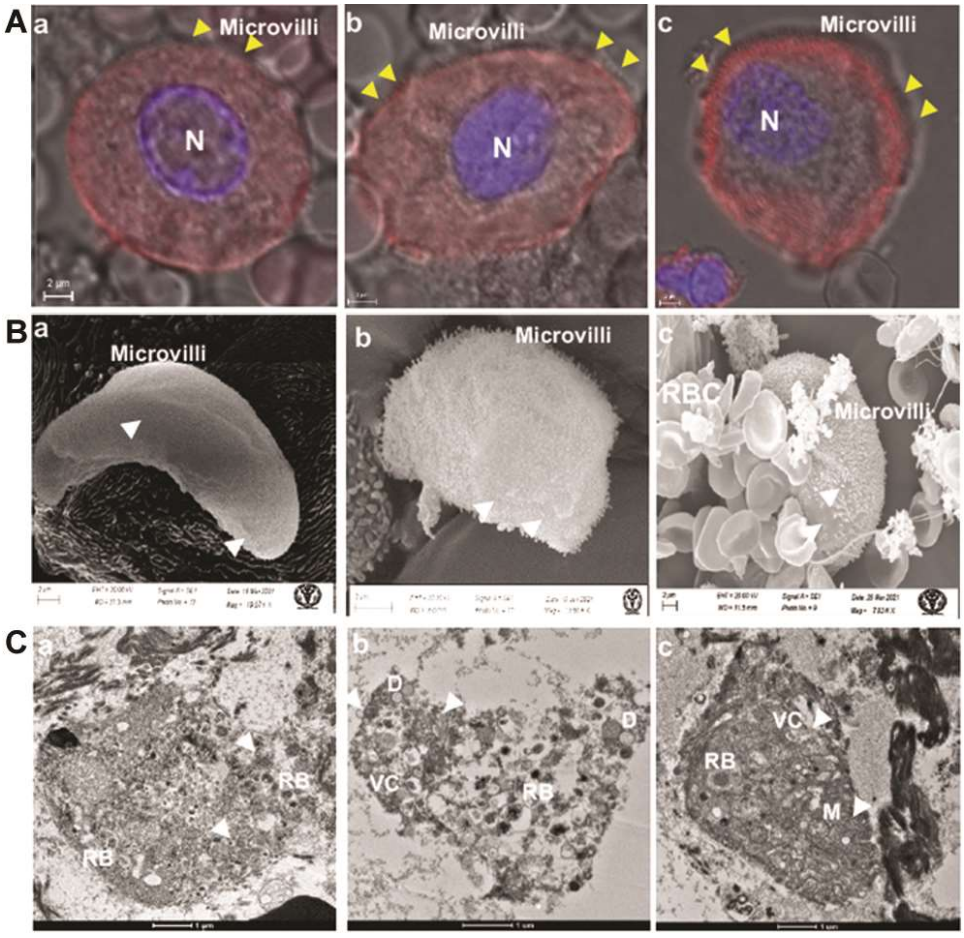

Fig. 4 — Ultrastructural detail of type II pneumocytes of BALF of COVID-19 patients using (A) Immunofluorescence study; (B) Scanning Electron Microscopy study; and (C) Transmission Electron Microscopy study. The IF study confirms the level of infection, and the SEM study confirms the different shapes of microvilli. TEM study reveals the presence of different size lamellar bodies and damage in the ultrastructure, such as cytoplasmic vacuolization and many electron-dense bodies. Mv: Microvilli; N: Nucleus; VC: Viral compartment; D: Double membrane vesicle; M: Mitochondria; RB: Residual body; white arrowhead indicates the virus

patients, suggesting that these cells may play a crucial role in the clearance of virus particles from the lungs. There was an increase in the number of lipid bodies and many prominent pseudopodia, indicating the activation of macrophages[19] (Fig. 5). The increased presence of apoptotic macrophages in BALF suggests that these immune cells actively participate in the host antiviral defense mechanisms during severe SARS-CoV-2 infection. The increased number of apoptotic macrophages could result from the virus's pathogenicity, host & immune response, or a combination of both.

Neutrophils

Neutrophils are important innate immune system cells and play a crucial role in cellular defence against infectious agents. The ultrastructural changes in the infiltrated neutrophil cells from BALF samples of severely infected COVID-19 patients were microscopically investigated. Neutrophil cells were identified based on their characteristic multilobulated

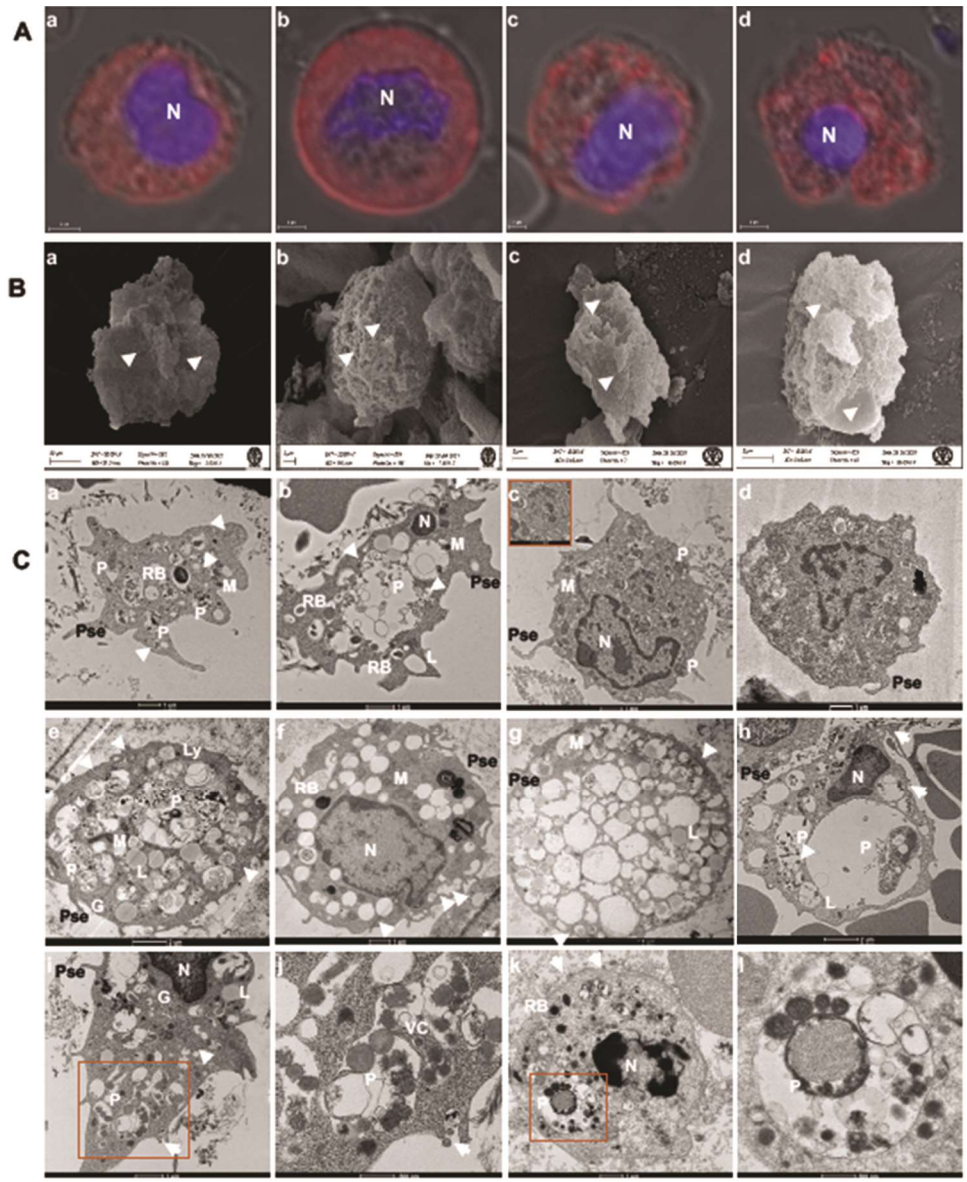

Fig. 5 — Ultrastructural imaging of the alveolar macrophage cells from the BALF of severe COVID-19 patients. These cells showed distinctive morphology in (A) Immunofluorescence study with a dense and distorted nucleus with viral S protein-specific protein; (B) The SEM imaging revealed the rough and fibrous surface along with the virus-like particles; and (C) Transmission Electron Microscopy shows the morphology of the macrophage (a, b, c, d), activated cells with characteristic lipid bodies (e, f, g, h), and enlarged view of phagosomes (i, j, k, l). Pse: Pseudopodia; N: Nucleus; G: Golgi complex; VC: Viral compartment; L:Lipid Body; P:Phagosomes; M: Mitochondria; RB: Residual body; white arrowhead indicates the virus

nuclei and cytoplasmic granules. Our immunofluorescence study revealed that these cells displayed distinct morphological and ultrastructural changes compared with healthy individuals (Fig. 6 A).

In COVID-19 patients, we observed significant ultrastructural changes, such as increased cytoplasmic granularity and vacuolization, indicating their activation and phagocytic activity. This suggests the essential role of these cells in combating viral invasion. We also observed the presence of extracellular traps (NETs) released by neutrophils, which can lead to tissue damage and lunginflammation[30]. The observed nuclear lobulation and cytoplasmic vacuolization suggest activation of stress-induced apoptosis, which has also been reported in other viral infections[31]. The release of extracellular traps (NETs) by neutrophils is a defence mechanism against viruses. However, although NETs play a crucial role in trapping and neutralizing pathogens, they can also lead to tissue damage and lung inflammation, exacerbating respiratory complications in COVID-19 patients[32,33]. The nuclear lobulation and cytoplasmic vacuolization indicate stress-induced apoptosis in neutrophils during Severe SARS-CoV-2 infection. This has been reported in other viral infections and suggests that the immune response against the virus can activate programmed cell death pathways in neutrophils[34,35].

In the SEM images, neutrophils appeared a round/oval shape with a rough surface (Fig. 6B). In contrast, neutrophils from severely infected COVID-19 patients showed marked surface ultrastructural changes, such as irregular and rough surfaces, loss of surface protrusions and blebs, formation of extracellular traps, and irregular surface morphology (Fig. 6B). We also observed the presence of SARS-CoV-2 virus particles attached to the

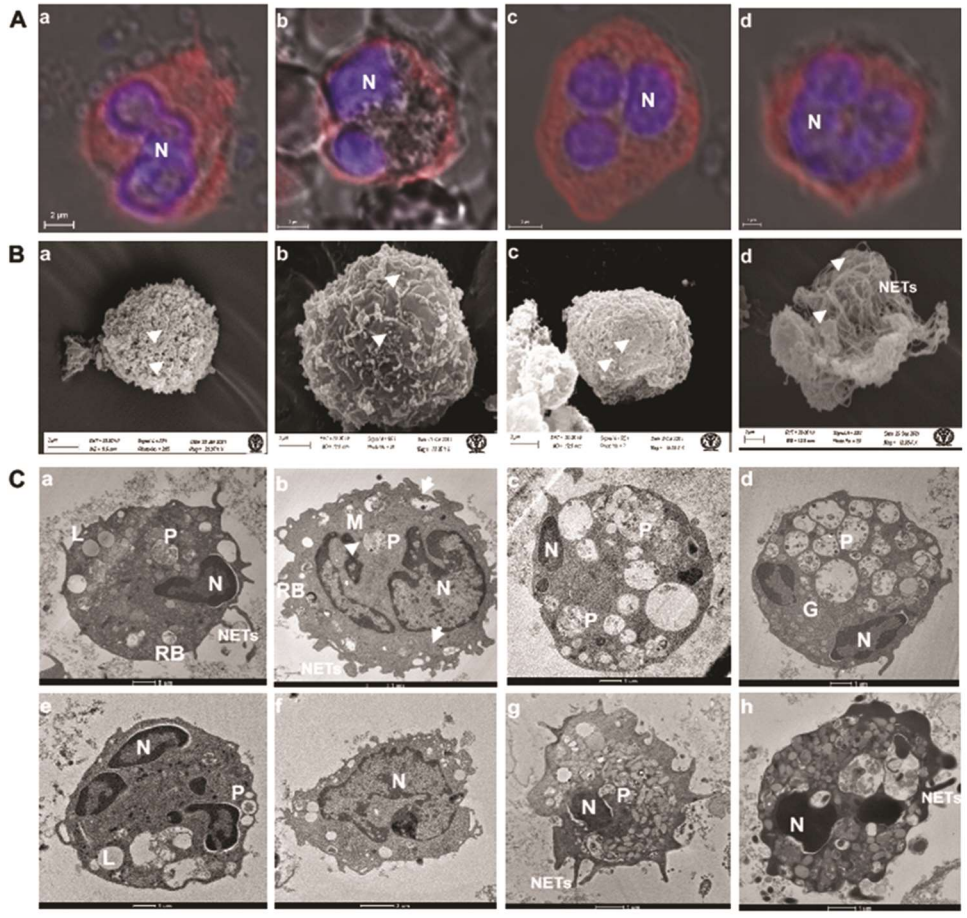

Fig. 6 — Ultrastructural analysis of Neutrophils using (A) Immunofluorescence; (B) Scanning Electron Microscopy; and (C) Transmission Electron Microscope. IF study confirms the activation of neutrophils with plenty of neutrophils extracellular traps (NETs) with distorted multilobed nuclei, which were also identified in SEM and TEM studies. Increased cytoplasmic granularity and vacuolization, indicating their activation and phagocytic activity. N: Nucleus; NETs : Neutrophils Extracellular Traps M: Mitochondria; G: Golgi Complex; P: Phagosomes; RB: Residual body; white arrowhead indicates the virus

surface, suggesting a role for these cells in viral clearance and the immune response (Fig. 6B).

In TEM imaging, neutrophils from COVID-19 patients showed nuclear lobulation and cytoplasmic vacuolization, which were not observed in the healthy individual (Fig. 6C). The increased number of cytoplasmic granules reflects their role in phagocytosis and the release of proinflammatory cytokines. These changes may contribute to the dysregulated immune response and tissue damage observed in patients with severe COVID-19. We observed the presence of membrane-bound extracellular traps and the formation of cytoplasmic vacuoles, often containing cellular debris (Fig. 6C).

Conclusion

We thank all patients' relatives for permitting us to collect BALF from the patients. This work was supported by grants from the IUSSTF Indo-US Virtual Network for the COVID-19 program (IUSSTF/VN- COVID/007/2020). Other funding by DBT (BT/INF/22/SP44285/2021), ICMR, SERB, and AIIMS intramural grants is acknowledged. SAIF-AIIMS New Delhi is acknowledged as the imaging facility for the SEM and TEM. DST-FIST confocal microscope facility is also acknowledged for the facility for Immunofluorescence. We acknowledged Dr. Kapil Soni and Prof. Anjan Trikha for permission to collect the BALF samples from the respective wards.

Acknowledgement

We thank all patients' relatives for permitting us to collect BALF from the patients. This work was supported by grants from the IUSSTF Indo-US Virtual Network for the COVID-19 program (IUSSTF/VN- COVID/007/2020). Other funding by DBT (BT/INF/22/SP44285/2021), ICMR, SERB, and AIIMS intramural grants is acknowledged. SAIF-AIIMS New Delhi is acknowledged as the imaging facility for the SEM and TEM. DST-FIST confocal microscope facility is also acknowledged for the facility for Immunofluorescence. We acknowledged Dr. Kapil Soni and Prof. Anjan Trikha for permission to collect the BALF samples from the respective wards.

Conflict of interest

All authors declare no conflict of interest.

References

1 Pollard CA, Morran MP & Nestor-Kalinoski AL, The COVID-19 pandemic: a global health crisis. *Physiol Genomics*, 52 (2020) 549.

2 Salzberger B, Buder F, Lampl B, Ehrenstein B, Hitzenbichler F, Holzmann T, Schmidt B & Hanses F, Epidemiology of SARS-CoV-2. *Infection*, 49 (2021) 233.

3 Sohrabi C, Alsafi Z, O'Neill N, Khan M, Kerwan A, Al-Jabir A, Iosifidis C & Agha R, World Health Organization declares global emergency: A review of the 2019 novel coronavirus (COVID-19). *Int J Surg*, 76 (2020) 71.

4 Guan WJ, Ni ZY, Hu Y, Liang WH, Ou CQ, He JX, Liu L, Shan H, Lei CL, Hui DSC,Du B, Li LJ, Zeng G, Yuen KY, Chen RC, Tang CL, Wang T, Chen PY, Xiang J, Li SY, Wang JL, Liang ZJ, Peng YX, Wei L, Liu Y, Hu YH, Peng P, Wang JM, Liu JY, Chen Z, Li G, Zheng ZJ, Qiu, SQ, Luo J, Ye CJ, Zhu SY & Zhong NS, Clinical Characteristics of Coronavirus Disease 2019 in China. *N Engl J Med*, 382 (2020) 1708.

5 Huang C, Wang Y, Li X, Ren L, Zhao J, Hu Y, Zhang L, Fan G, Xu J, Gu X, Cheng Z, Yu T, Xia J, Wei Y, Wu W, Xie X, Yin W, Li H, Liu M, Xiao Y, Gao H, Guo L, Xie J, Wang G, Jiang R, Gao Z, Jin Q, Wang J & Cao B, Clinical features of patients infected with 2019 novel coronavirus in Wuhan, China. *Lancet*, 395 (2020) 497.

6 Zhou F, Yu T, Du R, Fan G, Liu Y, Liu Z, Xiang J, Wang Y, Song B, Gu X, Guan L, Wei Y, Li H, Wu X, Xu J, Tu S, Zhang Y, Chen H & Cao B, Clinical course and risk factors for mortality of adult inpatients with COVID-19 in Wuhan, China: a retrospective cohort study. *Lancet*, 395 (2020) 1054.

7 Tian S, Xiong Y, Liu H, Niu L, Guo J, Liao M & Xiao SY, Pathological study of the 2019 novel coronavirus disease (COVID-19) through postmortem core biopsies. *Mod Pathol*, 33 (2020) 1007.

8 Xu Z, Shi L, Wang Y, Zhang J, Huang L, Zhang C, Liu S, Zhao P, Liu H, Zhu L, Tai Y, Bai C, Gao T, Song J, Xia P, Dong J, Zhao J & Wang FS, Pathological findings of COVID-19 associated with acute respiratory distress syndrome. *Lancet Respir Med*, 8 (2020) 420.

9 Mohapatra SK & Mukhopadhyay S, Host response to SARS-CoV-2: Insight from transcriptomic studies. *Indian J Biochem Biophys*, 58 (2021) 7.

10 Pandit K, Gupta S & Sharma AG, Clinico-Pathogenesis of COVID-19 in children. *Indian J Biochem Biophys,* 57 (2020) 264.

11 Santana MF, Pinto RAA, Marcon BH, Medeiros L, Morais T, Dias LC, Souza LP, Melo GC, Monteiro WM, Lacerda MVG, Val FA, Lalwani PJ & Ferreira LCL, Pathological findings and morphologic correlation of the lungs of autopsied patients with SARS-CoV-2 infection in the Brazilian Amazon using transmission electron microscopy. *Rev Soc Bras Med Trop*, 54 (2021) e0850.

12 Su WL, Lu KC, Chan CY & Chao YC, COVID-19 and the lungs: A review. *J Infect Public Health*, 14 (2021) 1708.

13 Bradley BT, Maioli H, Johnston R, Chaudhry I, Fink SL, Xu H, Najafian B, Deutsch G, Lacy JM, Williams T, Yarid N & Marshall DA, Histopathology and ultrastructural findings of fatal COVID-19 infections in Washington State: a case series. *Lancet*, 396 (2020) 320.

14 Parchwani D, Trivedi D, Bhatt A, Dholariya S, Chaudhari SP & Pathak M, Global research trends of interleukin-6 in SARS-CoV-2 infection. *Indian J Biochem Biophys*, 528 (2022) 528.

15 Yang MS, Oh BK, Yang D, Oh EY, Kim Y, Kang KW, Lim CW, Koh GY, Lee SM & Kim B, Ultra- and micro-structural changes of respiratory tracts in SARS-CoV-2 infected Syrian hamsters. *Vet Res*, 52 (2021) 121.

16 Baron A, Hachem M, Tran Van Nhieu J, Botterel F, Fourati S, Carteaux G, De Prost N, Maitre B, Mekontso-Dessap A & Schlemmer F, Bronchoalveolar lavage in patients with COVID-19 with invasive mechanical ventilation for acute respiratory distress syndrome. *Ann Am Thorac Soc*, 18 (2021) 723.
17 Gelarden I, Nguyen J, Gao J, Chen Q, Morales-Nebreda L, Wunderink R, Li L, Chmiel JS, Hrisinko M, Marszalek L, Momnani S, Patel P, Sumugod R, Chao Q, Jennings LJ, Gembower TR, Ji P & Chen YH, Comprehensive evaluation of bronchoalveolar lavage from patients with severe COVID-19 and correlation with clinical outcomes. *Hum Pathol*, 113 (2021) 92.
18 Ray PS & Goswami B, COVID-19 and Hyperinflammatory Syndrome. *Indian J Biochem Biophys,* 57 (2020) 662.
19 Chaudhary S, Rai P, Joshi A, Yadav P, Sesham K, Kumar S, Mridha AR, Baitha U, Nag TC, Soni KD, Trikha A & Yadav SC, Ultracellular Imaging of Bronchoalveolar Lavage from Young COVID-19 Patients with Comorbidities Showed Greater SARS-COV-2 Infection but Lesser Ultrastructural Damage Than the Older Patients. *Microsc Microanal*, 6 (2022) 1.
20 Chaudhary S, Rai P, Sesham K, Kumar S, Singh P, Nag TC, Chaudhuri P, Trikha A & Yadav SC, Microscopic imaging of bronchoalveolar fluids of COVID-19 positive intubated patients reveals the different level of SARS-CoV-2 infection on oral squamosal epithelial cells. *Indian J Biochem Biophys*, 58 (2021) 196.
21 Chaudhary S, Yadav R, Kumar S & Yadav S, Ultrastructural study confirms the formation of single and heterotypic syncytial cells in bronchoalveolar fluids of COVID-19 patients. *Virol J,* 20 (2023) 97.
22 Snijder EJ, Limpens R, de Wilde AH, de Jong AWM, Zevenhoven-Dobbe JC, Maier HJ, Faas F, Koster AJ & Barcena M, A unifying structural and functional model of the coronavirus replication organelle: Tracking down RNA synthesis. *PLoS Biol*, 18 (2020) e3000715.
23 V'Kovski P, Kratzel A, Steiner S, Stalder H & Thiel V, Coronavirus biology and replication: implications for SARS-CoV-2. *Nat Rev Microbiol*, 19 (2021) 155.
24 Klein S, Cortese M, Winter SL, Wachsmuth-Melm M, Neufeldt CJ, Cerikan B, Stanifer ML, Boulant S, Bartenschlager R & Chlanda P, SARS-CoV-2 structure and replication characterized by *in situ* cryo-electron tomography. *Nat Commun*, 11 (2020) 5885.
25 Ghosh S, Dellibovi-Ragheb TA, Kerviel A, Pak E, Qiu Q, Fisher M, Takvorian PM, Bleck C, Hsu VW, Fehr AR, Perlman S, Achar SR, Straus MR, Whittaker GR, de Haan CAM, Kehrl J, Altan-Bonnet G & Altan-Bonnet N, beta-Coronaviruses Use Lysosomes for Egress Instead of the Biosynthetic Secretory Pathway. *Cell*, 183 (2020) 1520.
26 Zhu N, Wang W, Liu Z, Liang C, Wang W, Ye F, Huang B, Zhao L, Wang H, Zhou W, Deng Y, Mao L, Su C, Qiang G, Jiang T, Zhao J, Wu G, Song J & Tan W, Morphogenesis and cytopathic effect of SARS-CoV-2 infection in human airway epithelial cells. *Nat Commun*, 11 (2020) 3910.
27 Pinto AL, Rai RK, Brown JC, Griffin P, Edgar JR, Shah A, Singanayagam A, Hogg C, Barclay WS, Futter CE & Burgoyne T, Ultrastructural insight into SARS-CoV-2 entry and budding in human airway epithelium. *Nat Commun*, 13 (2022) 1609.
28 Zhao J, Zhou H, Huang W, Zhou J, Qiu M, Deng Z, Chen L, Weng Y, Cai L, Gu Y Zheng Q, Chen Q, Hou X, Wang L, Shen L & Yang Z, Cell morphological analysis of SARS-CoV-2 infection by transmission electron microscopy. *J Thorac Dis*,12 (2020) 4368.
29 Chaudhary S, Yadav RP, Kumar S, Yadav SC, Aplastic anemia patients with severe COVID-19 showed abnormal ultrastructure features on type II pneumocytes of lungs. *Indian J Biochem Biophys*, 60 (2023) : in Press.
30 Radermecker C, Detrembleur N, Guiot J, Cavalier E, Henket M, d'Emal C, Vanwinge C, Cataldo D, Oury C, Delvenne P & Marichal T, Neutrophil extracellular traps infiltrate the lung airway, interstitial, and vascular compartments in severe COVID-19. *J Exp Med*, 217 (2020) e20201012.
31 Shubin AV, Demidyuk IV, Komissarov AA, Rafieva LM & Kostrov SV, Cytoplasmic vacuolization in cell death and survival. *Oncotarget*, 7 (2016) 55863.
32 Middleton EA, He XY, Denorme F, Campbell RA, Ng D, Salvatore SP, Mostyka M, Baxter-Stoltzfus A, Borczuk AC, Loda M, Cody MJ, Manne BK, Portier I, Harris ES, Petrey AC, Beswick EJ, Caulin AF, Iovino A, Abegglen LM, Weyrich AS, Rondina MT, Egeblad M, Schiffman JD & Yost CC, Neutrophil extracellular traps contribute to immunothrombosis in COVID-19 acute respiratory distress syndrome. *Blood*, 136 (2020) 1169.
33 Zuo Y, Yalavarthi S, Shi H, Gockman K, Zuo M, Madison JA, Blair C, Weber A, Barnes BJ, Egeblad M, Woods RJ, Kanthi Y & Knight JS, Neutrophil extracellular traps in COVID-19. *JCI Insight*, 5 (2020) e138999.
34 Elbim C, Katsikis PD & Estaquier J, Neutrophil apoptosis during viral infections. *Open Virol J*, 3 (2009) 52.
35 Ma Y, Zhang Y & Zhu L, Role of neutrophils in acute viral infection. *Immun Inflamm Dis*, 9 (2021) 1186.